Intraparticle Energy Transfer and Fluorescence Photoconversion in Nanoparticles: An Optical Highlighter Nanoprobe for Two-Photon Bioimaging

Sehoon Kim,[†] Heng Huang,[†,‡] Haridas E. Pudavar,[†] Yiping Cui,[‡] and Paras N. Prasad*[,†]

Institute for Lasers, Photonics and Biophotonics, Department of Chemistry, State University of New York, Buffalo, New York 14260-3000, and Advanced Photonics Center, Southeast University, Nanjing, China 210096

Received May 10, 2007

We report organically modified silica nanoparticles co-encapsulating two-photon fluorescent dye aggregates and a red-fluorescent energy acceptor, where the latter is indirectly excited through intraparticle energy transfer following two-photon excitation of the former. In vitro two-photon microscopy has demonstrated that these nanoprobes are avidly internalized into cells with bright acceptor fluorescence and that cellular optical highlighting is effected with red-to-green photoconversion by selective acceptor bleaching, while keeping the donor and the nanostructure of particles intact.

Introduction

Recent advances in imaging technology have enabled real-time monitoring of biochemical processes in cell biology, including protein trafficking, organelle dynamics, and cell lineage or moving within a developing organism etc.[1] The development of various laser scanning microscopy (LSM) techniques such as fluorescence resonance energy transfer (FRET) imaging,[2] fluorescence recovery after photobleaching (FRAP),[3] fluorescence loss in photobleaching (FLIP),[3] and fluorescence lifetime imaging (FLIM)[4] has enabled the study of molecular interactions and mobility of biomolecules in live cells. One such advanced imaging technique that is finding a wide range of applications in biology is "optical highlighting".[5] Optical highlighting is a method used to differentially highlight cells, organelles, or a specific population of proteins in cells for tracking them in time and space. Its common applications include the study of organelle dynamics, protein mobility measurements, cell signaling mechanisms, and cell lineage studies. Optical highlighting is accomplished by labeling the object of interest with photoactivatable or photoconvertible probes whose fluorescence is generated or color-changed by selective light irradiation. Optical highlighter probes, explored to date in the study of living cells, are generally classified into caged fluorescent molecules[6] and fluorescent protein variants.[5c,7] They are also useful for fluorescence photoactivation localization microscopy, a recently developed optical imaging method with nanometer resolution.[8] Multiphoton-induced photoactivation and photoconversion have also been studied to take advantage of three-dimensionally localized excitation.[6b−c,9] Here, we report a nanophotonics approach to a novel photoconvertible optical highlighter system and its application to two-photon laser scanning microscopy (TPLSM) which offers advantages such as sectioning ability, less phototoxicity, greater tissue penetration, better spatial resolution, less overall photobleaching, and less complication by autofluorescence.[1,10] This two-photon fluorescent

* To whom correspondence should be addressed. E-mail: pnprasad@buffalo.edu.

[†] State University of New York.

[‡] Southeast University.

(1) Prasad, P. N. *Introduction to Biophotonics*; John Wiley & Sons: Hoboken, NJ, 2003.

(2) (a) Politz, J. C. *Trends Cell Biol.* **1999**, *9*, 284. (b) Majoul, I.; Goroshkov, A.; Duden, R. In *Visions of the Cell Nucleus*; Hemmerich, P., Diekmann, S., Eds.; American Scientific Publishers: Valencia, CA, 2005; pp 239−247.

(3) Lippincott-Schwartz, J.; Snapp, E.; Kenworthy, A. *Nat. Rev. Mol. Cell Biol.* **2001**, *2*, 444.

(4) (a) Periasamy, A.; Wang, X. F.; Wodnick, P.; Gordon, G.; Kwon, S.; Diliberto, P. A.; Herman, B. *Microsc. Microanal.* **1995**, *1*, 13. (b) Elangovan, M.; Day, R. N.; Periasamy, A. *Proc. SPIE* **2002**, *4620*, 267.

(5) (a) Jakobs, S.; Schauss, A. C.; Hell, S. W. *FEBS Lett.* **2003**, *554*, 194. (b) Robinson, L. C.; Marchant, J. S. *Biophys. J.* **2005**, *88*, 1444. (c) Wiedenmann, J.; Nienhaus, G. U. *Expert Rev. Proteomics* **2006**, *3*, 361.

(6) (a) Politz, J. C. *Trends Cell Biol.* **1999**, *9*, 284. (b) Zhao, Y.; heng, Q.; Dakin, K.; Xu, K.; Martinez, M. L.; Li, W.-H. *J. Am. Chem. Soc.* **2004**, *126*, 4653. (c) Dakin, K.; Li, W.-H. *Nat. Methods* **2006**, *3*, 959.

(7) (a) Patterson, G. H.; Lippincott-Schwartz, J. *Science* **2002**, *297*, 1873. (b) Ando, R.; Hama, H.; Yamamoto-Hino, M.; Mizuno, H.; Miyawaki, A. *Proc. Natl. Acad. Sci. U.S.A.* **2002**, *99*, 12651. (c) Chudakov, D. M.; Belousov, V. V.; Zaraisky, A. G.; Novoselov, V. V.; Staroverov, D. B.; Zorov, D. B.; Lukyanov, S.; Lukyanov, K. A. *Nat. Biotechnol.* **2003**, *21*, 191. (d) Chudakov, D. M.; Verkhusha, V. V.; Staroverov, D. B.; Souslova, E. A.; Lukyanov, S.; Lukyanov, K. A. *Nat. Biotechnol.* **2004**, *22*, 1435. (e) Wiedenmann, J.; Ivanchenko, S.; Oswald, F.; Schmitt, F.; Röcker, C.; Salih, A.; Spindler, K.-D.; Nienhaus, U. *Proc. Natl. Acad. Sci. U.S.A.* **2004**, *101*, 15905.

(8) (a) Betzig, E.; Patterson, G. H.; Sougrat, R.; Lindwasser, O. W.; Olenych, S.; Bonifacino, J. S.; Davidson, M. W.; Lippincott-Schwartz, J.; Hess, H. F. *Science* **2006**, *313*, 1642. (b) Hess, S. T.; Girirajan, T. P. K.; Mason, M. D. *Biophys. J.* **2006**, *91*, 4258.

(9) (a) Marchant, J. S.; Stutzmann, G. E.; Leissring, M. A.; LaFerla, F. M.; Parker, I. *Nat. Biotechnol.* **2001**, *19*, 645. (b) Post, J. N.; Lidke, K. A.; Rieger, B.; Arndt-Jovin, D. J. *FEBS Lett.* **2005**, *579*, 325. (c) Schneider, M.; Barozzi, S.; Testa, I.; Faretta, M.; Diaspro, A. *Biophys. J.* **2005**, *89*, 1346.

(10) (a) Pawley, J. B. *Handbook of Biological Confocal Microscopy*; Plenum Press: New York, 1995. (b) Denk, W.; Strickler, J. H.; Webb, W. W. *Science* **1990**, *248*, 73. (c) Helmchen, F.; Denk, W. *Nat. Methods* **2005**, *2*, 932.

10.1021/cm071273x CCC: $37.00
Published on Web 10/24/2007

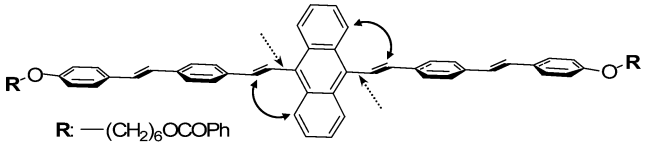

BDSAO

Figure 1. Chemical structure of BDSAO. The hydrogens inducing internal steric hindrance and the distorted bonds are indicated by the solid and the dotted arrows, respectively.

optical highlighter nanoprobe utilizes aggregation-enhanced fluorescence, nanoscopic intraparticle energy transfer, and selective acceptor bleaching in donor−acceptor co-encapsulating organically modified silica (ORMOSIL) nanoparticles.

ORMOSIL nanoparticles have proven to be biocompatible[11] and stable without releasing encapsulated hydrophobic molecules.[12] In this study, we have co-encapsulated in ORMOSIL nanoparticles a small amount of Nile Red as a red-fluorescent energy acceptor and an excess amount of energy up-converting donor, BDSAO (Figure 1), to produce efficient energy transfer. BDSAO is a green-fluorescent, alkoxy-substituted variant of a 9,10-bis[4′-(4″-aminostyryl)-styryl]anthracene derivative (BDSA) which has been developed by us as a special class of hydrophobic dye exhibiting aggregation-enhanced two-photon absorption (TPA) and fluorescence.[13] As in the case of BDSA, BDSAO shows weak fluorescence in solution ($\Phi_f \sim 0.03$) whereas it is intensified upon nanoaggregation ($\Phi_f = 0.18-0.29$, see Figure S1 in Supporting Information), which is in contrast to the fluorescence quenching of common organic dyes at high concentration or in the aggregated state.[14] As shown in Figure 1, in the isolated molecule state, the π-conjugated framework is severely distorted with free torsional motion which leads to a severe reduction in the quantum yield. In the aggregated state, this torsional motion is considerably reduced by loose packing of partially planarized dyes, leading to a significant increase in quantum yield.[13] Also, improved delocalization of the π-electrons in the partially planarized geometry produces an increase in two-photon absorption.[13] This aggregation-enhanced fluorescence offers an opportunity to prepare dye-concentrated nanoparticles, enabling excess loading of donor in nanoparticles while retaining the fluorescing capability, which provides an optimal condition for efficient collection and harvest of photon energy. Recently, we have proved this concept by showing that the fluorescent aggregates of BDSA, formed by phase separation in ORMOSIL nanoparticles at high loading concentration, can act as an efficient energy up-converting donor for near-IR energy transfer to the co-encapsulated photosensitizer for photodynamic therapy.[15]

Scheme 1. Synthetic Procedures for BDSAO

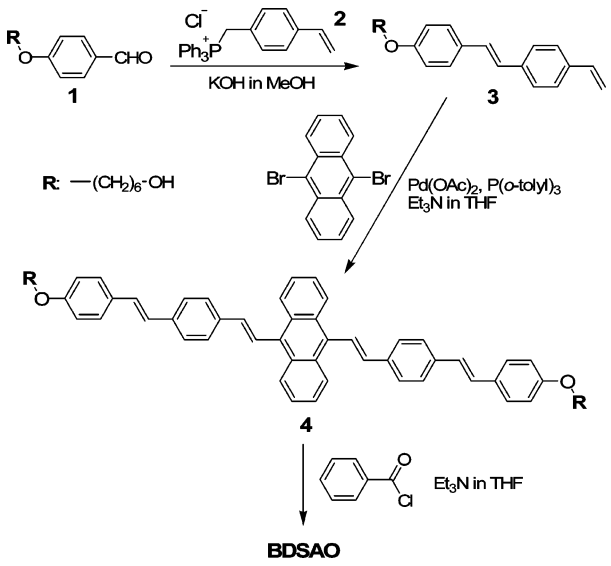

Experimental Section

Chemical structures were identified by ^{1}H NMR (Varian INOVA-400, 400 MHz) and electrospray ionization (ESI) mass spectra (Themo Finnigan LCQ Advantage mass spectrometer). Cosurfactant 1-butanol and NH_4OH (28.0−30.0%) are products of J. T. Baker. All other chemicals used were purchased from Aldrich. BDSAO was synthesized following the procedures depicted in Scheme 1. UV−vis absorption and one-photon excited fluorescence were measured using a Shimadzu UV-3600 spectrophotometer and a Jobin-Yvon Fluorog FL-311 spectrofluorometer, respectively.

4-(4-{6-Hydroxyhexyloxy}styryl)styrene (3). Potassium hydroxide (1.9 g, 33.9 mmol) in methanol (20 mL) was added dropwise to a solution of 4-(6-hydroxyhexyloxy)benzaldehyde[16a] (**1**, 5 g, 22.5 mmol) and 4-vinylbenzyltriphenylphosphonium chloride[16b] (**2**, 11.2 g, 27 mmol) in methanol (60 mL). The reaction mixture was stirred at room temperature for 1 day and filtered to give a pure *trans*-isomer precipitate selectively. The filtered product was further washed with cold methanol several times. Yield: 2.9 g (40%). ^{1}H NMR (400 MHz, DMSO-d_6): δ 7.84−7.63 (m, 6H), 7.40 (d, 1H, $J = 16.4$ Hz), 7.27 (d, 1H, $J = 16.4$ Hz), 7.12 (d, 2H, $J = 8.7$ Hz), 6.92 (dd, 1H, $J = 17.4$, 11.1 Hz), 6.03 (d, 1H, $J = 17.4$ Hz), 5.44 (d, 1H, $J = 11.1$ Hz), 4.57 (t, 1H, $J = 4.8$ Hz), 4.17 (t, 2H, $J = 6.5$ Hz), 3.58 (m, 2H), 2.0−1.8 (m, 2H), 1.7−1.5 (m, 6H). MS (ESI): calcd for $C_{22}H_{26}O_2$, $m/z = 341.21$ ($M + H_3O^+$); found, $m/z = 341.7$ ($M + H_3O^+$).

9,10-Bis(4-{4-[6-benzoyloxyhexyloxy]styryl}styryl)-anthracene (BDSAO). A mixture of **3** (1.5 g, 4.65 mmol), 9,10-dibromoanthracene (0.62 g, 1.85 mmol), $Pd(OAc)_2$ (60 mg), tri-*o*-tolylphosphine (180 mg), triethylamine (4 mL), and tetrahydrofuran (THF, 26 mL) in a pressure tube was stirred at 80 °C under argon

(11) (a) Shimada, M.; Shoji, N.; Takahashi, A. *Anticancer Res.* **1995**, *15*, 109. (b) Lal, M.; Levy, L.; Kim, K. S.; He, G. S.; Wang, X.; Min, Y. H.; Pakatchi, S.; Prasad, P. N. *Chem. Mater.* **2000**, *12*, 2632. (c) Roy, I.; Ohulchanskyy, T. Y.; Pudavar, H. E.; Bergey, E. J.; Oseroff, A. R.; Morgan, J.; Dougherty, T. J.; Prasad, P. N. *J. Am. Chem. Soc.* **2003**, *125*, 7860. (d) Zhao, X.; Bagwe, R. P.; Tan, W. *Adv. Mater.* **2004**, *16*, 173. (e) Bharali, D. J.; Klejbor, I.; Stachowiak, E. K.; Dutta, P.; Roy, I.; Kaur, N.; Bergey, E. J.; Prasad, P. N.; Stachowiak, M. K. *Proc. Natl. Acad. Sci. U.S.A.* **2005**, *102*, 11539.

(12) (a) Jain, T. K.; Roy, I.; De, T. K.; Maitra, A. N. *J. Am. Chem. Soc.* **1998**, *120*, 11092. (b) Roy, I.; Ohulchanskyy, T. Y.; Bharali, D. J.; Pudavar, H. E.; Mistretta, R. A.; Kaur, N.; Prasad, P. N. *Proc. Natl. Acad. Sci. U.S.A.* **2005**, *102*, 279.

(13) Kim, S.; Zheng, Q.; He, G. S.; Bharali, D. J.; Pudavar, H. E.; Baev, A.; Prasad, P. N. *Adv. Funct. Mater.* **2006**, *16*, 2317.

(14) Birks, J. B. In *Photophysics of Aromatic Molecules*; Wiley: London, 1970.

(15) Kim, S.; Ohulchanskyy, T. Y.; Pudavar, H. E.; Pandey, R. K.; Prasad, P. N. *J. Am. Chem. Soc.* **2007**, *129*, 2669.

(16) (a) Gangadhara; Kishore, K. *Macromolecules* **1995**, *28*, 806. (b) Bazan, G. C.; Oldham, W. J., Jr.; Lachicotte, R. J.; Tretiak, S.; Chernyak, V.; Mukamel, S. *J. Am. Chem. Soc.* **1998**, *120*, 9188.

atmosphere for 1 day. The cooled reaction mixture was poured into ethyl acetate and stored in a freezer for 2 h. The filtered precipitate was dissolved in a minimal amount of *N*-methyl-2-pyrrolidinone (NMP), and the insoluble part was removed by filtration. After pouring the mixture into diethyl ether, the precipitate was filtered and dried, to give a crude product of 9,10-bis(4-{4-[6-hydroxyhexyloxy]-styryl}styryl)anthracene (**4**, 0.53 g, 35%) which was pure enough for the next step, as judged by thin layer chromatography. To a solution of **4** (0.2 g, 0.24 mmol) in THF (10 mL) and triethylamine (1 mL), benzoyl chloride (0.2 g, 1.42 mmol) was added slowly in an ice bath. The reaction mixture was slowly heated and refluxed for 1 h. After cooling, the mixture was poured into water and extracted with dichloromethane two times. The collected organic phase was dried with $MgSO_4$ and the solvent was evaporated at reduced pressure. The residue was purified by column chromatography on a silica gel. The eluting impurities were removed using dichloromethane/*n*-hexane (1/1 by volume) and then the product was collected by eluting with dichloromethane. Yield 0.058 g (23%). ^{1}H NMR (400 MHz, $CDCl_3$): δ 8.42 (q, 4H), 8.06 (d, 4H, $J = 8.0$ Hz), 7.95 (d, 2H, $J = 16.8$ Hz), 7.67 (d, 4H, $J = 8.4$ Hz), 7.58 (d, 4H, $J = 8.4$ Hz), 7.54−7.40 (m, 14H), 7.14 (d, 2H, $J = 16.2$ Hz), 7.04 (d, 2H, $J = 16.2$ Hz), 6.94 (d, 2H, $J = 16.8$ Hz), 6.91 (d, 4H, $J = 8.8$ Hz), 4.35 (t, 4H, $J = 6.4$ Hz), 4.01 (t, 4H, $J = 6.4$ Hz), 1.9−1.5 (m, 16H). MS (ESI): calcd for $C_{72}H_{66}O_6$, $m/z = 1045.51$ ($M + H_3O^+$), 1027.50 ($M + H^+$), 940.48 ($M + H_3O^+ -$ benzoyl), 922.47 ($M + H^+ -$ benzoyl); found, $m/z = 1044.9$ ($M + H_3O^+$), 1027.8 ($M + H^+$), 940.5 ($M + H_3O^+ -$ benzoyl), 922.3 ($M + H^+ -$ benzoyl).

Preparation of Dye-Encapsulating ORMOSIL Nanoparticles. The nanoparticles, entrapping either one or both of Nile Red and BDSAO, were synthesized by coprecipitating the dyes with polymeric organically modified silica sol in the nonpolar core of Aerosol OT (AOT)/1-butanol micelles in deionized water. NMP was used as a hydrophilic solvent which has unlimited water miscibility as well as suitable solubility for both Nile Red and BDSAO. To obtain a clear solution of prepolymerized silica sol, 0.2 g of triethoxyvinylsilane (VTES) in 2 mL of NMP was hydrolyzed and condensed in the presence of 40 μL of NH_4OH at room temperature for 12 h to 1 day, until adding one drop of the resulting solution into excess pure water made white bulk precipitate without liquid phase of unreacted VTES or oligomers. After syringe filtering by membrane filter (0.2 μm pore size), 0.15 mL of the sol solution was homogeneously mixed with 0.57 mL of NMP solutions containing either or both Nile Red (0.05 mg; 0.4 wt % loading with respect to the added VTES amount) and BDSAO (1.36 mg; 10 wt % loading). The micelles were prepared by dissolving 0.22 g of AOT and 0.4 mL of 1-butanol in 10 mL of deionized water. Nanoprecipitation was induced by one-shot syringe injection of the above NMP solutions (0.6 mL) into the prepared micelle dispersions under vigorous magnetic stirring. The resulting mixtures were further stirred at room temperature, to ensure completion of sol−gel condensation within the coprecipitated nanoparticles. After 1 day of stirring, AOT and 1-butanol were removed by dialyzing the dispersion against deionized water in a 12−14 kDa cutoff cellulose membrane for 48 h.

Cell Culture and Nanoparticle Uptake. HeLa (human cervix epitheloid carcinoma) cells from American Type Culture Collection, Manassas, VA, were cultured in a Minimum Essential Medium (MEM) supplemented with 10% fetal bovine serum (FBS), following the supplier's instruction. For nanoparticle uptake, cells plated in 35 mm glass bottom Petri dishes were treated with co-encapsulating nanoparticle (NP-AD) dispersion and incubated at 37 °C (5% CO_2) for 1 h.

Confocal and Two-Photon Microscopy. A Leica TCS SP2-AOBS confocal system mounted on an inverted microscope was used for all imaging, FRET analyses, and other microscopic measurements. This microscope is equipped with multiple visible laser lines (405, 442, 458, 476, 488, 514, 543, and 633 nm) for visible excitation for confocal imaging as well as a Ti:sapphire laser (Mira from Cohrent Inc., tunable from 740 to 980 nm, 140 fs pulse width, 76 MHz repetition rate) for multiphoton excitation. The power under the microscope was controlled using neutral density filters and was maintained at 10 mW for two-photon imaging. A 63× oil immersion objective (HCX PL APO CS 63× NA 1.40) was used for all imaging studies. The fluorescence signal was collected by the same objective and was sent to two independent PMT (R6357, Hamamatsu)-based detectors through a confocal aperture (completely open aperture for two-photon imaging) and a prism-based spectrometer. The spectrally tunable filters on two separate imaging channels were set for donor (500−550 nm) and acceptor (620−740 nm) emissions.

Optical Highlighting Using Acceptor Bleaching. Acceptor of the selected region of interest (ROI) was irreversibly bleached and the increase of fluorescence signal in the donor channel was recorded. Before bleaching, a pulsed diode laser (405 nm, repetition rate 10 MHz) was used for exciting and recording single-photon donor fluorescence and the 543 nm line from the HeNe laser was used for recording acceptor fluorescence images. In the case of two-photon imaging, a Ti:sapphire laser tuned to 800 nm was used for excitation of the donor fluorescence, and the confocal aperture was left completely open for maximal signal collection efficiency. During acceptor bleaching processes, the selected ROIs were scanned repeatedly (20 frames) with the 543 nm line from the HeNe laser at full power. Postbleaching images were acquired by reverting back to the prebleaching imaging settings for both donor and acceptor channels. As a control, acceptor bleaching experiments were done on cells labeled with NP-D (10 wt % BDSAO encapsulated in ORMOSIL) and NP-A (0.4 wt % Nile Red encapsulated in ORMOSIL). In both cases, no enhancement of signal in the donor channel was observed.

Fluorescence Lifetime Imaging (FLIM). For FLIM measurements, time-correlated single-photon counting (TCSPC) technique was used with a Becker & Hickl SPC-830 unit. A Hamamatsu H7422 PMT was attached to the X1 port (an external port adapter in the Leica TCS-SP2 system for sending the fluorescence signal after the confocal aperture into an external detector) through which the fluorescence signals were sent to the SPC-830 unit. This configuration was capable of performing lifetime measurements as well as imaging using both single-photon excitation (pulsed diode laser source) and two-photon excitation. Additional filters in the signal path were used to cut off excitation as well as to select specific fluorescence channels. In this study to measure the BDSAO fluorescence lifetime as well as to obtain lifetime images of BDSAO channel (donor), we used a customized band-pass filter HQ550/80 (Chroma) in front of the detector. All images were acquired at a 128×128 resolution and typical integration time for a single image was less than 10 min. The instrument response function (IRF) for single-photon measurements was generated by measuring the fluorescence lifetime of a dye with known lifetime (10 μM solution of PRL-L1 dye[17] with a known life time of 55 ps from Streak camera-based measurements). For two-photon measurements, the IRF was generated using second-harmonic generation (SHG) from urea crystals. The obtained lifetime data was analyzed by iterative

(17) He, G. S.; Lin, T.-C.; Chung, S.-J.; Zheng, Q.; Lu, C.; Cui, Y.; Prasad, P. N. *J. Opt. Soc. Am. B* **2005**, *22*, 2219.

reconvolution with the IRF using SPCImage (Becker &Hickl) software.

Nanoprobe Mobility Measurements in Cell. FRAP experiments were done immediately after acceptor bleaching of selected ROIs. Two channel images were taken with given time intervals (3 s × 20 frames + 15 s × 20 frames + 60 s × 20 frames) after bleaching of acceptor (thus, the recovery of donor fluorescence from energy-transfer mechanisms). The donor channel is used to monitor the gradual loss of donor fluorescence due to diffusion of the acceptor-bleached nanoparticles into neighboring areas, and the acceptor channel is used to monitor the recovery of acceptor fluorescence due to diffusion of unbleached nanoparticles into the bleached area. A decay curve of donor fluorescence and a recovery curve of acceptor fluorescence were obtained after nonlinear curve fitting using a double-exponential decay function.

Results and Discussion

Dye-encapsulating ORMOSIL nanoparticles were prepared with a homogeneous mixture of dyes and prepolymerized triethoxyvinylsilane (VTES) sol in a hydrophilic solvent, *N*-methyl-2-pyrrolidinone (NMP). Dye encapsulation was accomplished through transient emulsification of the solution in the nonpolar interior of aqueous Aerosol OT (AOT) micelles and spontaneous coprecipitation via a "solvent displacement" process, i.e., diffusive depletion of NMP into the aqueous exterior.[18] Loading concentrations of dyes in ORMOSIL nanoparticles (defined as [dye/VTES] by weight) were chosen as follows: 0.4 wt % of Nile Red for the acceptor-alone sample (NP-A), 10 wt % of BDSAO for the donor-alone sample (NP-D), and 0.4 wt % Nile Red/10 wt % BDSAO for the acceptor−donor co-encapsulating sample (NP-AD). Although the nanoparticles obtained by this method are polydispersed in size, the average diameters were controlled to be less than 30 nm, as estimated by transmission electron microscopic (TEM) images (see Figure S2 in Supporting Information), which are small enough to minimize disturbance of normal cellular physiology and to keep the spatial separation between the donor and the acceptor molecules within the range of fluorescence resonance energy transfer (FRET). After removal of anionic surfactant (AOT) by dialysis against deionized water, all the nanoparticle samples showed a moderate negative ζ potential at pH 7.0 (see Figure S3 in Supporting Information), indicating that the dispersions in water are stabilized by the negative surface charge. It is noted that the nanoparticles containing an excess amount of BDSAO have a larger size and a more negative ζ potential than the acceptor-alone sample: NP-A (23.3 nm, −21.3 mV), NP-D (25.4 nm, −37.0 mV), and NP-AD (25.8 nm, −37.3 mV). The tendency of ζ potential (more negative with excess loading of BDSAO) is attributable to the increased surface hydrophobicity by the presence of excess BDSAO and subsequently promoted preferential adsorption of anions (OH^- or residual AOT), which has been suggested to explain the negative surface charge of non-ionogenic hydrophobic colloids.[19]

Figure 2a shows spectral matching for energy transfer, between Nile Red and BDSAO in water-dispersed ORMOSIL nanoparticles. The acceptor-alone nanoparticle sample, NP-A, exhibits typical Nile Red fluorescence with a peak at 640 nm ($\Phi_f \sim 0.3$), indicating that by coprecipitation with polymeric VTES sol, the hydrophobic Nile Red molecules at the loading concentration of 0.4 wt % have successfully been embedded in the particle matrix, with minimal self-aggregation or interaction with water. Note that the Nile Red fluorescence is completely quenched in water dispersions by self-aggregation.[20] In contrast, 10 wt % of BDSAO in NP-D forms aggregate domains in the particle matrix by phase separation, to emit characteristic green fluorescence of the aggregate state. Importantly, this aggregate emission of BDSAO is spectrally matched well with the absorption of Nile Red in NP-A, which allows for energy transfer between them when co-encapsulated in ORMOSIL nanoparticles, as in the case of NP-AD.

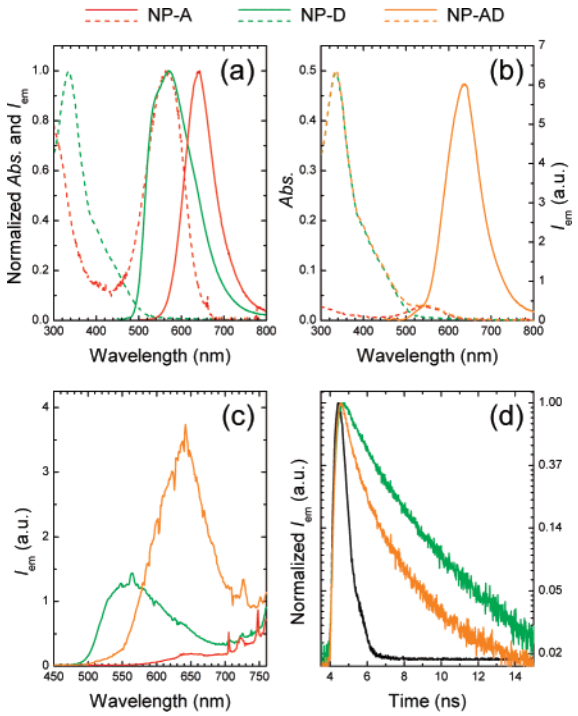

Figure 2. Optical properties of water-dispersed ORMOSIL nanoparticles encapsulating: 0.4 wt % Nile Red (NP-A), 10 wt % BDSAO (NP-D), and 0.4 wt % Nile Red/10 wt % BDSAO (NP-AD). The wavelengths for one- and two-photon excitations are 430 and 800 nm, respectively. (a) Normalized absorption (dashed) and one-photon fluorescence emission (solid) of NP-A and NP-D. (b) Absorption (dashed) and one-photon fluorescence emission (solid) of NP-AD, plotted with absorptions (dashed) of the same amount of NP-A and NP-D. (c) Two-photon fluorescence emission from the same amount of NP-A, NP-D, and NP-AD. (d) Donor fluorescence (BDSAO component) decay of two-photon-excited NP-D and NP-AD. The black line indicates instrument response function (IRF).

Linear absorption and fluorescence spectra of the co-encapsulating sample, NP-AD, are shown in Figure 2b. The absorption spectrum is composed of the contributions from each component, i.e., a simple superposition of a small amount of Nile Red and an excess amount of BDSAO,

(18) Horn, D.; Rieger, J. *Angew. Chem., Int. Ed.* **2001**, *40*, 4331.

(19) (a) Jordan, D. O.; Taylor, A. J. *Trans. Faraday Soc.* **1952**, *48*, 346. (b) Voeglti, L. P.; Zukoski, C. F. *J. Colloid Interface Sci.* **1991**, *141*, 92. (c) Dunstan, D. E. *J. Chem. Soc. Faraday Trans.* **1993**, *89*, 521. (d) Litton, G. M.; Olson, T. M. *J. Colloid Interface Sci.* **1994**, *165*, 522. (e) Schechter, R. S.; Garcia, A.; Lachaise, J. *J. Colloid Interface Sci.* **1998**, *204*, 398.

(20) Jiang, J.; Tong, X.; Zhao, Y. *J. Am. Chem. Soc*. **2005**, *127*, 8290.

suggesting no ground-state interaction between them. However, its fluorescence spectrum resembles that of Nile Red in NP-A, with significant quenching of the fluorescence from excess BDSAO. This quenching interaction supports that donor and acceptor exist in the same nanoparticle space by co-encapsulation. It is noted in NP-AD that the Nile Red absorption at the excitation wavelength of 430 nm is minimal, compared with that of BDSAO. Consequently, the quenching of BDSAO fluorescence indicates that the light energy collected by a large quantity of BDSAO is focused into a small quantity of Nile Red by efficient intraparticle energy transfer, to produce a considerable amplification of the acceptor fluorescence by indirect excitation.

The indirect excitation through energy transfer is still valid under two-photon excitation conditions because the BDSAO aggregates have approximately 1 order of magnitude larger TPA cross section (σ_2) than Nile Red. The σ_2 values of the BDSAO nanoaggregate dispersion in water and Nile Red solution in 1,4-dioxane were estimated to be 40.5 and 4.3 GM, respectively, by the two-photon-induced fluorescence method,[21] using a femtosecond Ti-sapphire laser at 800 nm and a Rhodamine 6G solution in methanol as a reference.[21b] Figure 2c shows fluorescence emission from NP-A, NP-D, and NP-AD, under 800 nm excitation, where the initial feed weights of VTES were kept constant for a quantitative comparison. It is clearly seen that the strong two-photon fluorescence of excess BDSAO (NP-D) is reduced by ~89% in the presence of Nile Red (NP-AD), as in the case of Figure 2b (see Figure S4 in Supporting Information). Moreover, when compared with directly two-photon-excited Nile Red in NP-A, its fluorescence component in NP-AD is ~30 times amplified by indirect two-photon excitation, indicating that two-photon energy is efficiently up-converted by co-encapsulated excess BDSAO and harvested into Nile Red by intraparticle energy transfer.

To examine the nature of intraparticle energy transfer, the fluorescence lifetime of BDSAO was measured for NP-D and NP-AD, under two-photon excitation at 800 nm. In both cases, the fluorescence kinetics of BDSAO were found to be best fitted by a biexponential decay, as in the case of an amino-substituted variant, BDSA.[15] As shown in Figure 2d, the amplitude (pre-exponential factor)-averaged lifetime (τ_m)[22] of BDSAO was shortened from 1.4 ns (NP-D) to 820 ps (NP-AD), by co-encapsulation with Nile Red (see Supporting Information for the average lifetime calculation). From the reduction of donor lifetime, the efficiency of nonradiative energy transfer (FRET) is estimated to be ~48%, using the equation $1-\tau_{DA}/\tau_D$, where τ_{DA} and τ_D are the donor excited-state lifetime in the presence and absence of acceptor, respectively.[22] On comparison with the total energy-transfer efficiency (~89%) estimated from the fluorescence quenching of the donor (BDSAO) in Figure 2c, it is concluded that both radiative and nonradiative mechanisms are co-operative for the intraparticle energy transfer in the co-encapsulating nanoparticles (NP-AD).

Cellular uptake behavior of these nanoparticles was studied using a tumor cell line (HeLa, human cervix epitheloid carcinoma cells) and two-photon microscopy. The detailed procedures used for cell culture and nanoparticle uptake as well as for microscopy are given in the Experimental Section. Two-photon laser scanning fluorescence microscopy was performed using a confocal laser scanning microscope equipped with a Ti:sapphire laser (800 nm, 140 fs pulses, <10 mW under microscope). The spectrally tunable filters on two separate imaging channels were set for donor (500−550 nm) and acceptor (620−740 nm) emissions. These ORMOSIL nanoparticles were avidly taken up by tumor cells within 1 h incubation period, and cells showed bright fluorescence under confocal or two-photon microscopy. Figures 3a and 3b represent merged pseudocolor fluorescence images of HeLa cells treated with NP-AD for 1 h, taken under two-photon excitation (green, BDSAO/donor channel; red, Nile Red/acceptor channel). As in the case of water dispersion (Figure 2c), NP-AD inside cells showed bright two-photon fluorescence of Nile Red, with strong acceptor signal and minimal donor signal in each channel (column 1 of Figures 3a and 3b), indicating that the donor−acceptor co-encapsulating nanostructure remains intact in the cellular environment.

To demonstrate the cellular highlighting capability, we used repeated scanning with a 543 nm laser excitation, to photobleach the acceptor (Nile Red) in the selected areas of cells. It is to be noted that the coexisting donor (BDSAO) would be inert to the process of acceptor photobleaching because its absorption at 543 nm is minimal. Furthermore, the given photobleaching condition seems to have minimal phototoxic effect on the cell viability, as observed under microscopy. On photodestruction of Nile Red, the donor fluorescence increased significantly, as seen in column 2 of Figures 3a and 3b. With use of this acceptor bleaching technique, either a whole cell (Figure 3a) or part of a cell (Figure 3b) can be optically highlighted. From the donor fluorescence enhancement on acceptor depletion,[3,23] the average intraparticle energy-transfer efficiency of NP-AD inside cells was estimated as 87%. This intracellular value (for combined radiative and nonradiative transfer) is similar to that obtained in the aqueous dispension (Figure S4 in Supporting Information), further supporting the intracellular retention of co-encapsulating nanostructure. Confocal fluorescence lifetime imaging (CFLIM) was also conducted using a FLIM attachment utilizing a time-correlated single-photon counting unit (Becker & Hickl SPC-830). Figure 3c shows histograms of donor lifetime distribution in cells treated with nanoprobes containing donor in the absence and presence of acceptor (NP-D and NP-AD, respectively). The average donor lifetime change estimated from these FLIM images also shows a FRET efficiency of 47%, similar to that shown in aqueous dispersions (Figure 2d). This again confirms that the nanoparticle geometry is not altered on cellular entry, with minimal leakage of BDSAO or Nile Red molecules from the encapsulating nanoparticles.

(21) (a) Xu, C.; Webb, W. W. *J. Opt. Soc. Am. B* **1996**, *13*, 481. (b) Albota, M. A.; Xu, C.; Webb, W. W. *Appl. Opt.* **1998**, *37*, 7352.
(22) Valeur, B. *Molecular Fluorescence: Principles and Applications*; Wiley-VCH Verlag GmbH: Weinheim, 2001.
(23) Kenworthy, A. K. *Methods* **2001**, *24*, 289.

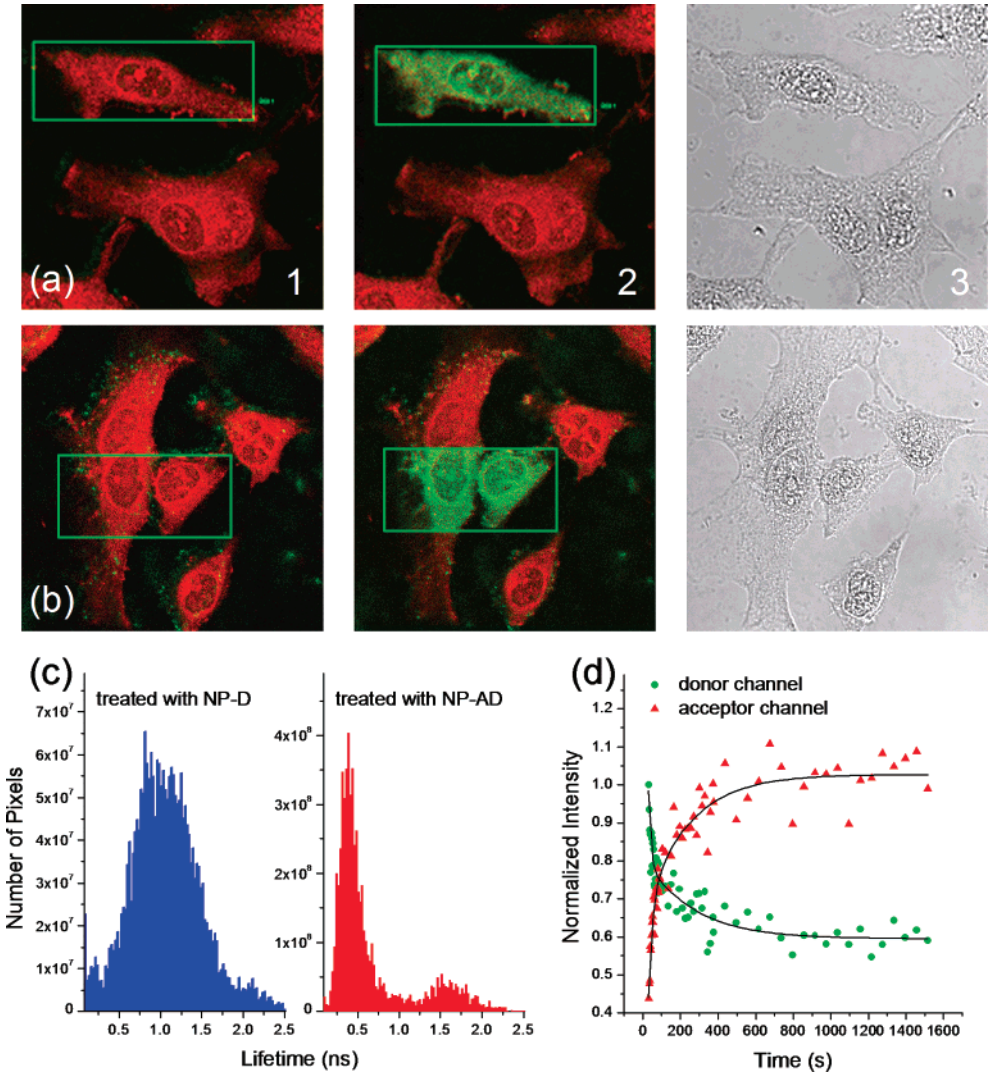

Figure 3. In vitro cell studies of ORMOSIL nanoparticles. (a, b) Pseudocolor donor (green)−acceptor (red) channel-merged two-photon fluorescence images of HeLa cells treated with NP-AD for 1 h, before (column 1) and after (column 2) acceptor bleaching in the areas indicated by green boxes. Column 3, transmission images. (c) Histograms showing average intraparticle lifetime distribution of donor (BDSAO) in cells treated with donor-containing nanoparticles (NP-D and NP-AD). (d). Fluorescence intensity profiles showing intracellular mobility of nanoparticles (NP-AD), monitored by temporal signal changes of both donor and acceptor channels in optically highlighted areas of cells. The black lines are best-fitted kinetic functions.

We have also confirmed that these nanoparticles are not destroyed during optical highlighting, by monitoring intracellular particle movement in time. As shown in Figure 3d, the temporal fluorescence change in the highlighted area of a cell was monitored to obtain the mobility of NP-AD. Due to the exchange of nanoprobes between the highlighted and unhighlighted areas of the cell, the acceptor channel signal increases by entry of acceptor-unbleached intact nanoprobes, while the donor channel signal decreases by exit of acceptor-bleached ones. The time constants ($t^{1/2}$, defined as the time at which the intensity drops/increases to half the maximum value) of the profiles in Figure 3d, estimated from the exponential curve fitting for acceptor signal increase ($t^{1/2} \sim 86$ s) and the donor signal decrease ($t^{1/2} \sim 92$ s), are comparable, confirming that during the process of optical highlighting, the acceptor-bleached nanoparticles keep their initial structure without destruction, to maintain a similar intracellular mobility to that of unbleached ones. This approach based on the photoconversion of fluorescence color can improve the accuracy of intracellular mobility measurements over the conventional FRAP method, which monitors only fluorescence recovery after photobleaching, by providing two simultaneous channels for monitoring the intensity changes.

Conclusions

We have developed a novel energy-transfer-based photoconvertible nanoprobe, which can be used for optical highlighting of entire cells or organelles/compartments of cells for two-photon fluorescence imaging. Efficient intraparticle energy transfer from an excess amount of BDSAO aggregates to Nile Red, co-encapsulated in ORMOSIL nanoparticles, was found to be attributed to the combined radiative and nonradiative mechanisms. Optical highlighting by significant fluorescence color change has been achieved by differential photobleaching of acceptor in the selected areas of cells. From the comparison between the extra- and the intracellular energy-transfer efficiencies, it has been concluded that these nanoparticles maintain their dye-encapsulating nanostructures inside cells and during optical highlighting processes, suggesting a potential as an intracellular probe. We have also demonstrated the advantages of

two-color optical highlighting over the conventional FRAP technique for intracellular mobility measurements.

Acknowledgment. This work was supported in part by a grant from the Directorate of Chemistry and Life Sciences of the Air Force Office of Scientific Research and in part by a grant from the National Institutes of Health (R01-CA119397).

Supporting Information Available: Optical properties of BDSAO, characteristic data of nanoparticles, intraparticle energy-transfer efficiency by two-photon excitation, and average lifetime calculation. This material is available free of charge via the Internet at http://pubs.acs.org.

CM071273X